Fast Exocytosis with Few Ca^{2+} Channels in Insulin-Secreting Mouse Pancreatic B Cells

Sebastian Barg,* Xiaosong Ma,* Lena Eliasson,* Juris Galvanovskis,* Sven O. Göpel,* Stefanie Obermüller,* Josef Platzer,† Erik Renström,* Michel Trus,‡ Daphne Atlas,‡ Jörg Striessnig,† and Patrik Rorsman*

*Department of Molecular and Cellular Physiology, Institute of Physiological Sciences, Lund University, BMC F11, SE-221 84 Lund, Sweden; †Institut für Biochemische Pharmakologie, Peter-Mayrstrasse 1, A-6020 Innsbruck, Austria; and ‡Department of Biological Chemistry, The Hebrew University of Jerusalem, 91904 Israel

ABSTRACT The association of L-type Ca^{2+} channels to the secretory granules and its functional significance to secretion was investigated in mouse pancreatic B cells. Nonstationary fluctuation analysis showed that the B cell is equipped with <500 $\alpha 1_C$ L-type Ca^{2+} channels, corresponding to a Ca^{2+} channel density of 0.9 channels per μm^2. Analysis of the kinetics of exocytosis during voltage-clamp depolarizations revealed an early component that reached a peak rate of 1.1 pFs^{-1} (≈650 granules/s) 25 ms after onset of the pulse and is completed within ~100 ms. This component represents a subset of ≈60 granules situated in the immediate vicinity of the L-type Ca^{2+} channels, corresponding to ~10% of the readily releasable pool of granules. Experiments involving photorelease of caged Ca^{2+} revealed that the rate of exocytosis was half-maximal at a cytoplasmic Ca^{2+} concentration of 17 μM, and concentrations >25 μM are required to attain the rate of exocytosis observed during voltage-clamp depolarizations. The rapid component of exocytosis was not affected by inclusion of millimolar concentrations of the Ca^{2+} buffer EGTA but abolished by addition of exogenous $L_{C753-893}$, the 140 amino acids of the cytoplasmic loop connecting the 2nd and 3rd transmembrane region of the $\alpha 1_C$ L-type Ca^{2+} channel, which has been proposed to tether the Ca^{2+} channels to the secretory granules. In keeping with the idea that secretion is determined by Ca^{2+} influx through individual Ca^{2+} channels, exocytosis triggered by brief (15 ms) depolarizations was enhanced 2.5-fold by the Ca^{2+} channel agonist BayK8644 and 3.5-fold by elevating extracellular Ca^{2+} from 2.6 to 10 mM. Recordings of single Ca^{2+} channel activity revealed that patches predominantly contained no channels or many active channels. We propose that several Ca^{2+} channels associate with a single granule thus forming a functional unit. This arrangement is important in a cell with few Ca^{2+} channels as it ensures maximum usage of the Ca^{2+} entering the cell while minimizing the influence of stochastic variations of the Ca^{2+} channel activity.

INTRODUCTION

The pancreatic B cell is electrically excitable and uses electrical signals to couple an elevation of the blood glucose concentration to insulin secretion (Ashcroft and Gribble, 1999). Insulin is released by Ca^{2+}-dependent exocytosis initiated by Ca^{2+} entering through voltage-gated L-type Ca^{2+} channels. Exocytosis in the B cell shares a number of features with neurotransmitter release in neurons. For example, many of the proteins (including the SNARE proteins VAMP, SNAP-25, syntaxin, and synaptotagmin) that regulate the release of neurotransmitters are present in the B cell and fulfill the same functions (for review, see Lang, 1999). There is also evidence that Ca^{2+} channels and secretory granules co-localize to the same part of the B cell suggesting a functional organization similar to that in the nerve terminal (Bokvist et al., 1995). Moreover, exocytosis is operational at cytoplasmic Ca^{2+} concentrations ($[Ca^{2+}]_i$) of several tens of micromolars (Takahashi et al., 1997), levels unlikely to be attained except in the close vicinity of the Ca^{2+} channels and much higher than those documented in pancreatic B cells by microfluorimetry (Grapengiesser et al., 1991; Ämmälä et al., 1993). The latter is probably an explanation to the observation that secretion in the B cell echoes Ca^{2+} channel activity and proceeds only during depolarization and stops immediately upon repolarization (Ämmälä et al., 1993). The B cell may represent an interesting example of Ca^{2+}-regulated secretion, as it is capable of high-speed exocytosis (500–600 granules/s) despite small Ca^{2+} current amplitudes (30–50 pA) (Gillis and Misler, 1992; Ämmälä et al., 1993). Although the exact number of Ca^{2+} channels in the B cell is not known, the magnitude of the whole-cell current suggests that the Ca^{2+} channel density is low, and hormone release must therefore be efficiently coupled to Ca^{2+} channel activity. We demonstrate here that the B cell contains fewer than 500 Ca^{2+} channels and propose that fast exocytosis in the B cell is achieved by the assembly of a complex of L-type Ca^{2+} channels and the secretory granules. Disassembly of this complex abolishes rapid exocytosis and results in a release pattern similar to that characterizing certain forms of human diabetes. We speculate that this organization, which ensures maximum usage of Ca^{2+} entering at minimal expenditure of metabolic energy to restore the resting $[Ca^{2+}]_i$, may have its counterpart in other excitable cells that need to be tonically active.

Received for publication 6 December 2000 and in final form 17 August 2001.

Address reprint requests to Patrik Rorsman, Department of Molecular and Cellular Physiology, Institute of Physiological Sciences, Lund University, BMC F11, SE-221 84 Lund, Sweden. Tel.:46-46-222-77-42; Fax: 46-46-222-77-63. E-mail: patrik.rorsman@mphy.lu.se.

0006-3495/01/12/3308/16 $2.00

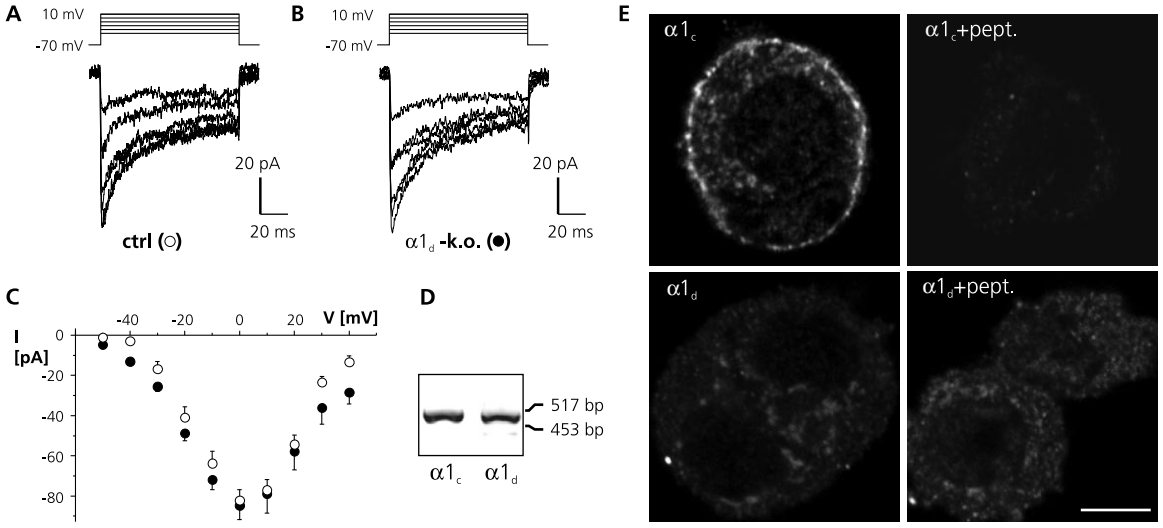

FIGURE 1 Mouse B cells contain $\alpha 1_C$ L-type Ca^{2+} channels. (*A* and *B*) Ca^{2+} currents evoked by membrane depolarizations from −70 mV to voltages between −40 mV and +10 mV (in 10 mV increments) in B cells from normal (*A*) and $\alpha 1_D$ knockout mice (*B*). The experiments were performed using the standard whole-cell configuration with the Cs^+-containing pipette solution (pipette solution III) and the standard extracellular solution containing 2.6 mM extracellular Ca^{2+} and 20 mM TEA. (*C*) Current (*I*)-voltage (*V*) relationships of L-type Ca^{2+} currents recorded from normal (○) and $\alpha 1_D$ knockout mice (●). Data are mean ± SE of 8 (○) and 11 (●) experiments. (*D*) RT-PCR analysis of islet mRNA using oligonucleotide probes against $\alpha 1_C$ (*left*) and $\alpha 1_D$ (*right*). (*E*) Immunofluorescence micrographs of B cells stained with antibodies against $\alpha 1_C$ (*upper left*) and $\alpha 1_D$ (*lower left*). The cells in the right panels were treated identically as the corresponding cells in the left panel, except that the antibodies were preincubated with the antigenic peptide used to raise the antibody. Scale bar = 5 μm.

MATERIALS AND METHODS

Preparation and culture of B cells

Mouse pancreatic B cells were isolated from NMRI-mice (Naval Medical Research Institute; purchased from Bomholtgaard, Ry, Denmark). In one series of experiments (Fig. 1 *B* and *C*), $\alpha 1_D$ null mice were used. The latter animals were generated in the Institute of Biochemical Pharmacology (Innsbruck, Austria) as described elsewhere (Platzer et al., 2000). The animals were killed by cervical dislocation and the pancreas quickly removed, followed by isolation of the pancreatic islets by collagenase digestion. The experimental procedures for sacrificing the animals were approved by the ethical committee at Lund University. The islets thus obtained were dissociated into single cells by vigorous shaking in Ca^{2+}-free solution and the resulting cell suspension was plated on Corning petri dishes or (for microfluorimetry) 22-mm glass coverslips. The cells were maintained in tissue culture for up to 2 days in RPMI 1640 medium containing 5 mM glucose, 10% (v/v) fetal calf serum, 100 μg/ml streptomycin, and 100 i.u./ml penicillin.

Electrophysiology

Patch electrodes were made from borosilicate glass capillaries coated with Sylgard close to the tips and fire-polished. The pipette resistance ranged between 2 and 4 MΩ when filled with the intracellular solutions specified below. The zero-current potential of the pipette was adjusted in the bath before giga-seal formation. Unless otherwise specified, all the electrophysiological experiments were conducted using the standard whole-cell configuration. In this recording mode, compounds are conveniently applied intracellularly by inclusion into the pipette solution dialyzing the cell interior. Exocytosis was elicited either by voltage-clamp depolarizations or photorelease of "caged" Ca^{2+} from Ca^{2+}-NP-EGTA preloaded into the cell. The electrophysiological recordings were performed using EPC-9 amplifiers and the Pulse software (version 8.30 or later; Heka Elektronik, Lambrecht, Germany).

Exocytosis was detected as changes in cell capacitance, which was estimated by the Lindau-Neher technique (Gillis, 1995) implementing the "Sine + DC" feature of the lock-in module. The amplitude of the sine wave was 20 mV and the frequency set as 500 Hz. Rapid depolarization-evoked capacitance increases with fast relaxation (within 1 ms, reflecting gating currents; Horrigan and Bookman, 1994) were rarely observed. In the few cases they did appear, the amplitude of the change in cell capacitance was measured once it had settled at a new steady-state level. It has been proposed (Takahashi et al., 1997) that release of γ-aminobutyrate (GABA)-containing synaptic-like microvesicles gives rise to a fast exocytotic component. Using an assay with sufficient sensitivity to detect exocytosis of individual GABA-containing vesicles, we were unable to document any release of GABA with a kinetics fast enough to give rise to the rapid changes in cell capacitance we describe here (Braun, Wendt, and Rorsman, manuscript in preparation). This conclusion is reinforced by the good correlation between the depolarization-evoked capacitance increases and amperometric detection of serotonin preloaded into the insulin-containing granules (Bokvist et al., 2000).

The number of Ca^{2+} channels per B cell was estimated from the tail currents that followed upon a 1.5-ms depolarization from −90 to +120 mV. The currents were filtered at 10 kHz and digitized at 40 kHz. The single-channel amplitude (i), the open probability (p_o), and the number of Ca^{2+} channels per cell (N) were then estimated by nonstationary fluctuation analysis as previously described (Heinemann and Conti, 1992) using PulseTools (Heka Elektronik).

Photorelease of caged Ca^{2+} or diazo-2 and measurements of $[Ca^{2+}]_i$

Photolysis of the Ca^{2+}-NP-EGTA complex or diazo-2 was effected by brief (<2 ms) flashes of ultraviolet (UV) light produced by an XF-10 flash photolysis apparatus (HiTech Scientific, Salisbury, UK). The efficiency of liberation was estimated to be 55% for NP-EGTA, and we assume the same efficiency for diazo-2.

$[Ca^{2+}]_i$ was measured by dual-excitation wavelength spectrofluorimetry using 50 μM of the low-affinity Ca^{2+}-indicators BTC or fura-FF (experiments involving photorelease of caged Ca^{2+}) or the high-affinity dye fura red (experiments using diazo-2; all from Molecular Probes, Eugene, OR). The measurements were conducted either on an IonOptix fluorescence imaging system (Milton, MA; measurements using fura red or BTC) or a PTI DeltaRam microfluorimetry system equipped with the software Felix (Monmouth Junction, NJ). The excitation and emission wavelengths were 340/380 and >505 nm for fura-FF and 420/490 and >515 nm for fura-red and BTC. The K_d-values for the Ca^{2+}-binding to fura-FF, fura-red, and BTC were taken as 35, 0.14, and 90 μM. The latter value is 13-fold higher than the value quoted by the manufacturer and derived by measuring the fluorescence ratio in droplets containing media with a composition similar to the pipette-filling solution in parallel with recordings of the free Ca^{2+} concentration using a Ca^{2+}-sensitive mini-electrode (Fluka, Milwaukee, WI). An equally high value for the K_d of BTC has been reported by others (Maeda et al., 1999). The fluorescence ratio was then converted into $[Ca^{2+}]_i$ using the equation of Grynkiewicz et al. (1985). In the BTC and fura-FF measurements, the fluorescence ratio recorded before photolysis was taken as the minimum and the value recorded shortly after rupturing the cell, by briefly clamping the membrane voltage to −500 mV, as the maximum.

Solutions

The extracellular solution consisted of 118 mM NaCl, 20 mM TEA-Cl, 5.6 mM KCl, 1.2 mM $MgCl_2$, 2.6 mM $CaCl_2$, 5 mM D-glucose, and 5 mM Hepes (pH 7.4 with NaOH). The pipette solution (pipette solution I) used in most experiments contained 125 mM Cs-glutamate, 10 mM CsCl, 10 mM NaCl, 1 mM $MgCl_2$, 0.05 mM EGTA, 3 mM Mg-ATP, 0.1 mM cAMP, 5 mM Hepes (pH 7.1 using CsOH). In the experiments involving photorelease of caged Ca^{2+}, the pipette solution (solution II) consisted of 110 mM K-glutamate, 10 mM KCl, 20 mM NaCl, 1 mM $MgCl_2$, 25 mM Hepes (pH 7.1 with KOH), 3 mM MgATP, 3 mM NP-EGTA (Molecular Probes), 2 mM $CaCl_2$, and 0.05 mM BTC or fura-FF. The initial $[Ca^{2+}]_i$ was estimated to be 0.3 μM assuming the same binding constants as for EGTA (Martell and Smith, 1974). In the experiments using diazo-2, the photoactivatable calcium-scavenger was added to intracellular solution I at a concentration of 0.3 mM. The effects of Ca^{2+} buffering on exocytosis were estimated by supplementing pipette solution I with 2 mM EGTA and 1 mM Ca^{2+} to produce free $[Ca^{2+}]_i$ of 233 nM. The synprint peptide (residues 753–893; $L_{c753-893}$) of the $\alpha1_C$-subunit of the L-type Ca^{2+} channel was included in the pipette solution (solution I) at a concentration of 2.5 μM. This sequence is 35% identical (43% including conservative changes) to the corresponding part of the $\alpha1_D$-subunit. The synprint peptide was prepared as described elsewhere (Wiser et al., 1999).

To increase Ca^{2+} channel amplitude and the open probability of the Ca^{2+} channels, the stationary fluctuation analysis was performed with an extracellular solution containing 110 mM $BaCl_2$ and 10 mM Hepes (pH 7.4 using NaOH). The pipette solution in these experiments (pipette solution III) consisted of 135 mM $CsCl_2$, 10 mM EGTA, 1 mM $MgCl_2$, 3 mM ATP-Mg, 0.1 mM cAMP, and 10 mM Hepes (pH 7.15 using CsOH). Both the intra- and extracellular media used in these experiments were supplemented with 1 μM (+)-BayK8644 (RBI, Natick, MA) to increase Ca^{2+} channel activity. The Ba^{2+}-containing solution was also used as the pipette solution in the single-channel measurements.

In recordings using the perforated patch whole-cell, the pipette solution consisted of 76 mM Cs_2SO_4, 10 mM CsCl, 10 mM KCl, 1 mM $MgCl_2$, and 5 mM Hepes (pH 7.35 with CsOH). Electrical contact with the cell interior was established by inclusion of the pore-forming antibiotic amphotericin B at a final concentration of 0.24 mg/ml in the pipette solution.

During the experiments the cells were was continuously superfused with the extracellular medium at a rate of 2 ml/min and the volume of the chamber reduced to 0.5 ml by a plastic insert. Except for the experiments used to estimate the number of Ca^{2+} channels per B cell, which were done at room temperature, all electrophysiological measurements were carried out at 32°C.

Reverse transcriptase PCR analysis of islet tissue

Poly-A mRNA was isolated from freshly prepared mouse islets using the Dynabeads mRNA DIRECT kit (Dynal Biotech, Oslo, Norway). Reverse transcriptase-polymerase chain reaction (RT-PCR; Superscript Reverse Transcriptase, Life Technologies) was then performed using poly-dT primers. The resulting cDNA was PCR probed (*Taq* DNA-Polymerase, Boehringer Mannheim, Basel) using primer sets against $\alpha1_C$ (forward 5′-GCACAAGACCTGCTACAACC and reverse 5′-AGGCTTGTCTTCATCCATGC) and $\alpha1_D$ (forward 5′-TCCTCCACATAGCCCTTTTG and reverse 5′-AGCCCTTGAGATCCTTCC).

Immunofluorescence microscopy

Islet cells were cultured on coverslips overnight, fixed in 4% formaldehyde (Polyscience, Warrington, PA) in phosphate-buffered saline, and permeabilized with 0.1% Triton X100. After blocking of nonspecific sites with 5% normal donkey serum, the cells were incubated overnight at 4°C with a 1:30 dilution of a rabbit anti-$\alpha1_C$ or rabbit anti-$\alpha1_D$ antibody (Alomone, Jerusalem, Israel). The cells were then incubated with a biotin-conjugated donkey-raised anti-rabbit antibody (Jackson Immuno, West Grove, PA) and finally labeled with streptavidin-Cy3. Immunofluorescence was studied on a Zeiss LSM510 confocal microscope using a 100×/1.4NA oil objective, the 543-nm excitation line, and >565-nm emission filter.

Data analysis

Data are quoted as mean ± SE of indicated number of experiments. Statistical significances were evaluated using Student's *t*-test.

RESULTS

B cell Ca^{2+} current flows through $\alpha1_C$ Ca^{2+} channels

Figure 1, *A* and *B* shows families of voltage-clamp current recorded at 2.6 mM extracellular Ca^{2+} upon depolarization from −70 mV to voltages between −50 mV and +40 mV in B cells isolated from normal NMRI- and $\alpha1_D$-null mice (Platzer et al., 2000). The peak Ca^{2+} current measured at 0 mV averaged −82 ± 5 pA (n = 8) and −84 ± 7 pA (n = 11) in NMRI- and the $\alpha1_D$-null mice, respectively. In control cells, the peak current was attained 3.7 ± 0.4 ms after onset of the depolarization and activation was equally rapid in the knockout B cells. The current (I)- voltage (V) relationships for the wild-type (○) and knockout mice (●) are shown in Fig. 1 *C*. It is clear that both the peak current amplitude and the voltage dependence overlap. Collectively, these data suggest that Ca^{2+} influx through $\alpha1_D$-containing L-type Ca^{2+} channels contributes little, if at all, to the Ca^{2+} current in mouse B cells. Indeed, we detected $\alpha1_C$, but not $\alpha1_D$ immunoreactivity in mouse B cells (Fig. 1 *E*). $\alpha1_D$ immunoreactivity was observed in a few islet cells with irregular morphology, which is very different from that of B cells that typically are round and have a diameter of 13 to 15 μm (Barg et al., 2000). RT-PCR analysis confirmed that islet cells express both $\alpha1_C$ and $\alpha1_D$ Ca^{2+}

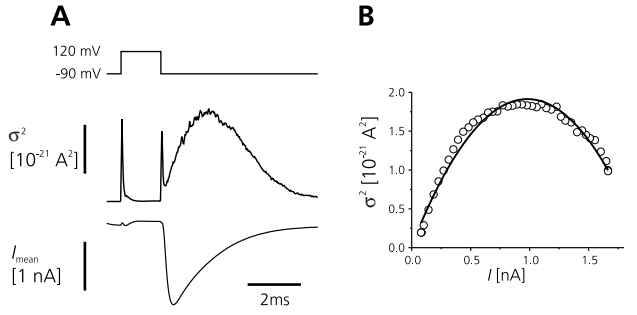

FIGURE 2 Low Ca^{2+} channel density in mouse B cells. (*A*) Variance (σ^2) and average of 325 sweeps of whole-cell currents (*I*) recorded during a depolarization from −90 mV to +120 mV. To increase *i* and p_o, the experiments were conducted with 110 mM Ba^{2+} as charge carrier and in the presence of 1 μM of the L-type Ca^{2+} channel agonist BayK8644. Note the large inward tail current upon stepping back to −90 mV. (*B*) Variance (σ^2) current (*I*) plot of the tail current in *A*. Eq. 1 was fitted to the data points yielding values of *N* and *i* of 495 channels and 3.96 pA, respectively.

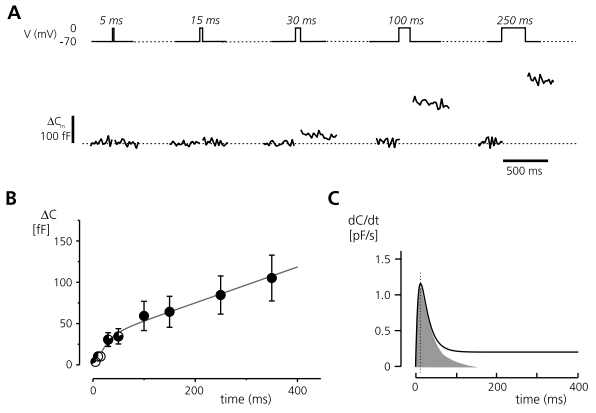

FIGURE 3 B cells contain ≈60 immediately releasable secretory granules. (*A*) Exocytotic responses (Δ*C*, *lower trace*) recorded from single B cells in response to depolarizations (*V*, *top trace*) to 0 mV of variable duration (5–450 ms, as indicated). The experiments were performed using the standard extracellular solution and pipette solution II. (*B*) Relationship between ΔC_m and duration of depolarization (*t*). Note that a substantial fraction of the total release occurs during the first 100 ms. The circles indicate the percentage responding cells. The number of responsive cells increased from 0% (○) during a 5-ms depolarization to 100% (●) during depolarizations ≥50 ms. Data are given as mean ± SE of 10 experiments. The curve is derived from Eq. 5. (*C*) Rate of exocytosis (d*C*/d*t*) estimated by derivation of the curve in *B*. The maximum exocytotic rate of 1.1 pF/s is attained 26 ms after onset of the depolarization. The gray area represents the fraction of total exocytosis that corresponds to the RRP (60 granules).

channels, the latter presumably reflecting the presence of cells other than insulin-secreting B cells in the islet (Fig. 1 *D*).

Ca^{2+} channel density in the B cell

The whole-cell Ca^{2+} current (*I*) is the product of the single-channel amplitude (*i*), the open probability (p_o), and the number of Ca^{2+} channels per B cell (*N*). The value of *N* was determined by nonstationary fluctuation analysis. The Ca^{2+} channels were activated by voltage-clamp depolarizations from −90 mV to +120 mV (Fig. 2 *A*). Although the latter voltage is much higher than that ever attained during spontaneous B cell electrical activity, such strong stimulation is useful because it can be expected to drive the Ca^{2+} channels into the maximally activated state. As +120 mV is beyond the reversal potential of the B cell Ca^{2+} current, the current is outward during the depolarization. However, when the membrane potential is stepped back to the holding potential, a large and rapidly deactivating tail current is observed. Fig. 2 *A* shows the average tail current (*I*) elicited by 325 depolarizations and its variance (σ^2). The relationship between *I* and σ^2 is shown in Fig. 2 *B*. The equation

$$\sigma^2 - \sigma_b^2 = i \times I - \frac{I^2}{N} \quad (1)$$

in which σ_b is the background variance before Ca^{2+} channel activation, was fitted to the data points yielding values of *N* and *i* of 454 ± 81 ($n = 5$) channels and 3.95 ± 0.04 pA ($n = 5$), respectively. Our value of *i* is in good agreement with that obtained from single-channel recordings under similar experimental conditions (Smith et al., 1993). In a cell with a surface area of 510 μm^2, as expected from the mean value of the cell capacitance of 5.1 ± 0.2 pF ($n = 64$) and assuming a specific membrane capacitance of 10 fF/μm^2, the value of *N* corresponds to a Ca^{2+} channel density of 0.9 ± 0.2 channels/μm^2.

Kinetics of depolarization-evoked exocytosis

For technical reasons, the time course of capacitance increase cannot be determined reliably during membrane depolarization. We therefore reconstructed the release kinetics by measuring the exocytotic responses elicited by progressively longer (5–450 ms) voltage-clamp depolarizations (Fig. 3). For depolarizations ≤15 ms, no consistent capacitance increases were detected. However, longer depolarizations evoked progressively larger responses, and the number of responsive cells increased from 33% at 15 ms and 67% at 30 ms to 100% for depolarizations lasting ≥50 ms (as indicated by open and filled circles in Fig. 3 *B*). These data are summarized in Fig. 3 *B* in which the amplitude of the exocytotic response is displayed against the duration of the depolarizing pulse.

Ca^{2+}-dependent exocytosis can, at least in the short term, be functionally divided into the release of granules from a readily releasable pool (RRP) and the subsequent refilling of the RRP from a reserve pool (RP; Heinemann et al., 1994; Voets et al., 1999). We hypothesized that this also applies to mouse pancreatic B cells and that secretion re-

flects the sequential release of the two pools of secretory granules according to the reaction scheme

$$RP \underset{k_{-1}}{\overset{k_1}{\rightleftharpoons}} RRP \xrightarrow{v_{exo}(t)} \text{exocytosis.} \quad (2)$$

We assume that only granules that have proceeded into RRP are capable of undergoing Ca^{2+}-dependent exocytosis (Voets, 2001). The supply of granules into RRP from RP is described by the rate k_1 and the reversal of the process is governed by the rate constant k_{-1}. Exocytosis proceeds at the speed $v_{exo}(t)$, which varies as a function of time after onset of depolarization (t). According to this model, the exchange of granules between RP and RRP and the release can be described by the equation

$$\frac{dp_2}{dt} = -k_{-1} \times p_2 - v_{exo} \times p_2 + k_1 \quad (3)$$

in which p_2 is the variable size of the RRP.

To take into account the local differences in $[Ca^{2+}]_i$ and thus in the rate of exocytosis during the first milliseconds of the depolarization, v_{exo} is approximated by a sigmoidal function

$$v_{exo} = \alpha_0 \times (1 - e^{-t/\tau}) \quad (4)$$

in which α_0 is the rate constant of exocytosis from the RRP and τ is the time constant for the sigmoidal part that describes the rate of exocytosis during the first milliseconds. Inserting this expression into Eq. 3 yields

$$\frac{dp_2}{dt} = -k_i \times p_2 - \alpha_0 \times (1 - e^{-t/\tau}) \times p_2 + k_1 \quad (5)$$

The size of the RRP, the rate k_1, the rate constants k_{-1} and α_0, and τ were determined by fitting Eq. 5 to the experimental data. In a series of 10 experiments, they averaged 98 ± 16 fF, 154 ± 48 fFs^{-1}, 0.44 ± 0.14 fFs^{-1}, 18 ± 9 s^{-1}, and 8.8 ± 2.6 ms. We point out that the above value of RRP represents a lower estimate because $[Ca^{2+}]_i$ is not uniform during channel mediated Ca^{2+} influx. From the rate constant of exocytosis α_0, the value of τ_0 (the time constant for release of RRP) can be estimated (i.e., ln $2/\alpha_0$) to be 41 ± 7 ms. The value of RRP equates to ≈60 secretory granules using a conversion factor of 1.7 fF per granule (Ämmälä et al., 1993). The value of k_1 suggests that 80 RP granules become available for release every second.

Figure 9 *C* shows how the exocytotic rate varies during depolarization. The time course is estimated by calculating the time derivative of the fit to Eq. 5. The maximum rate of exocytosis amounted 1.09 ± 0.36 pF/s and was attained 26 ± 6 ms after the onset of depolarization. The former value corresponds to the release of 640 granules per second and is in good agreement with those previously reported (Ämmälä et al., 1993). The gray area in Fig. 9 *C* corresponds to the fast component (RRP). It is clear that it is very short-lived and exhausted in ≈50 ms, a time span comparable with the duration of the B cell action potential (Ashcroft and Rorsman, 1989).

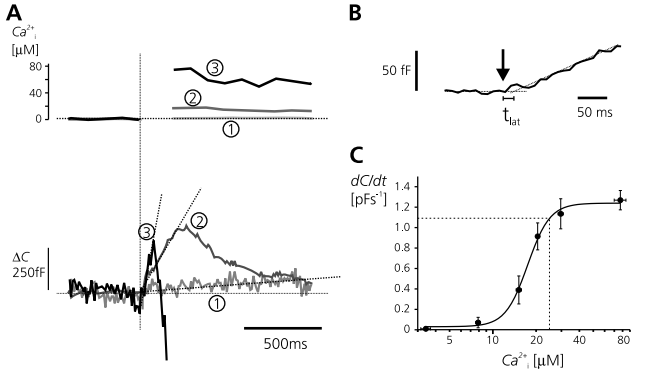

FIGURE 4 Ca^{2+}-dependent exocytosis in insulin-secreting cells operates at high $[Ca^{2+}]_i$. (*A*) Increase in $[Ca^{2+}]_i$ (*top*) and changes in cell capacitance (ΔC, *bottom*) upon photolysis of Ca^{2+}-NP-EGTA (effected at vertical line). The responses to low (*1*), intermediate (*2*), and high (*3*) $[Ca^{2+}]_i$ are shown. The initial rates of capacitance increase (d*C*/d*t*) are indicated by the dotted lines. The pipettes were filled with pipette solution II and the standard extracellular medium was used. (*B*) Delay between step increase of 45 μM in $[Ca^{2+}]_i$ (*arrow*) and detectable increase in cell capacitance (t_{lat}, 16 ms in this particular experiment). (*C*) Relationship between $[Ca^{2+}]_i$ and d*C*/d*t*. The solid line is the best fit to the Hill equation. Data from 60 experiments have been pooled. The dotted line indicates the maximum rate of exocytosis attained during a voltage-clamp depolarization (1.1 pF/s), which predicts a Ca^{2+} concentration at the release site of >25 μM.

$[Ca^{2+}]_i$ dependence of exocytosis in the B cell

Experiments using digital imaging of the $[Ca^{2+}]_i$-transient associated with depolarization-evoked exocytosis have revealed the existence of steep concentration gradients within the cell and that $[Ca^{2+}]_i$ close to the secretory granules approaches ≈10 μM (Bokvist et al., 1995). We have reanalyzed the Ca^{2+}-dependence of exocytosis by using photorelease of caged Ca^{2+} to produce instant and uniform step increases in $[Ca^{2+}]_i$. Fig. 4 *A* shows the increases in cell capacitance elicited by step increases in $[Ca^{2+}]_i$ to 4 , 20, and 70 μM. Exocytosis is slow at the lowest $[Ca^{2+}]_i$. At the two higher concentrations, endocytosis (seen as a decrease in membrane capacitance) supersedes exocytosis 100–500 ms after photorelease of Ca^{2+}. The dotted lines indicate approximate initial rates of exocytosis. Linear extrapolation back to the prestimulatory level indicated that there was a latency of 10 ± 3 ms between the UV flash and the initiation of exocytosis (ignoring an early component that probably represents a stimulation artifact due to UV irradiation) when $[Ca^{2+}]_i$ was 33 ± 12 μM (n = 7, Fig. 4 *B*); Ca^{2+} buffering during the initial 1.5 s is negligible but becomes prominent at later times (Eliasson et al., 1996; Gall et al., 1999). The relationship between $[Ca^{2+}]_i$ and the rate

of capacitance increase (dC_m/dt) in several cells ($n = 60$) is summarized in Fig. 4 *C*. Approximating the Hill equation to the data points indicated that exocytosis was half-maximal at 17.3 ± 0.5 μM $[Ca^{2+}]_i$. The Hill coefficient amounted to 5.3 ± 0.8, indicative of a high degree of cooperativity and is consistent with the idea that several Ca^{2+}-ions need to bind to the Ca^{2+}-sensor to initiate exocytosis. These values for the Ca^{2+}-dependence of exocytosis are in reasonable agreement with those previously reported (Takahashi et al., 1997) and much higher than the average (global) concentrations that can be measured using microfluorimetry (Ämmälä et al., 1993) and reinforce previous arguments that exocytosis is principally regulated by the Ca^{2+} concentration close to the Ca^{2+} channels. The maximum rate of exocytosis was 1.24 ± 0.4 pF/s and is achieved at $[Ca^{2+}]_i \geq 30$ μM. This rate of exocytosis is not too different from the maximum rate of exocytosis during voltage-clamp depolarizations (compare dotted lines in Figs. 3 *C* and 4 *C*). We therefore conclude that $[Ca^{2+}]_i$ at the release sites during Ca^{2+} channel openings must approach or even exceed 25 μM. We acknowledge that concomitant endocytosis at high $[Ca^{2+}]_i$ may lead to an apparent saturation of the exocytotic rate at falsely low $[Ca^{2+}]_i$. Unfortunately, it is not possible to selectively inhibit endocytosis. However, we believe that the initial rate of capacitance increase should provide a reasonable estimate of the release rate as endocytosis requires prior exocytosis and is relatively slow and initiated with a delay with respect to exocytosis (Eliasson et al., 1996). Nevertheless, the Ca^{2+}-dependence quoted above should be regarded as a lower estimate.

A subset of RRP is situated close to the Ca^{2+} channels

We explored the relationship between RRP and Ca^{2+} channels by combining voltage-clamp depolarizations and photorelease of caged Ca^{2+} (Fig. 5). Whereas the voltage-clamp depolarizations will preferentially release granules situated in the vicinity of the Ca^{2+} channel (immediately releasable pool (IRP) using the nomenclature of Voets et al., 1999), the spatially uniform elevation of $[Ca^{2+}]_i$ resulting from photolysis of NP-EGTA can be expected to release all RRP granules. The stimulation protocol consisted of a train of five 500-ms depolarizations from −70 mV to zero followed by flash photolysis of Ca^{2+}—NP-EGTA preloaded into the cell. The depolarizations evoked inactivating Ca^{2+} currents with a peak amplitude as low as ≈50 pA. It can be noted that there is no sign of exocytosis proceeding between the depolarizations after the two first pulses. It is only during the third and fourth depolarization, when measured $[Ca^{2+}]_i$ exceeds 3 μM, that exocytosis continues after repolarization and then at a rate of ≈50 fF/s. This rate of exocytosis is comparable with that attained during intracellular dialysis with a Ca^{2+} buffer with a free Ca^{2+} concentration of ≈2 μM (Barg et al., 2001). It can be observed that

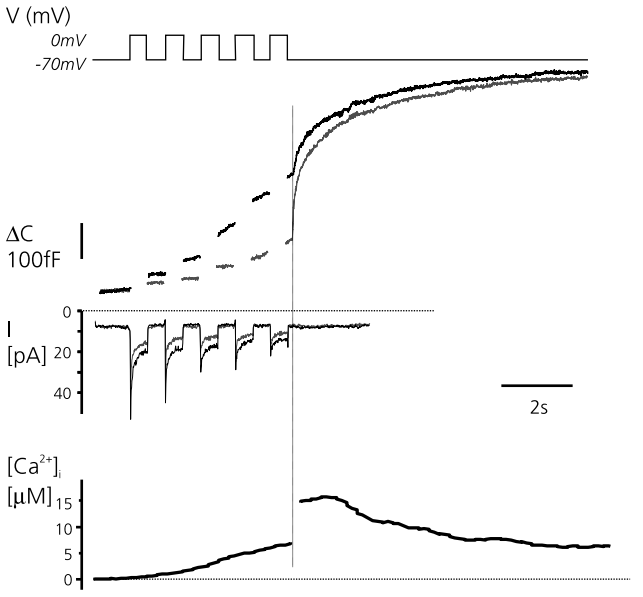

FIGURE 5 IRP is a subset of RRP. Exocytosis was triggered by a series of five 500-ms depolarizations from −70 to 0 mV applied at 1 s^{-1} (*V*, *top trace*) followed by photorelease of caged Ca^{2+} (200 ms after the last depolarization, *vertical line*). Whole-cell Ca^{2+} currents (*I*, *second trace from bottom*), the increase in cell capacitance (ΔC, *second from top*), and cytoplasmic Ca^{2+} ($[Ca^{2+}]_i$, *bottom*) were measured in parallel. The stimulation protocol was repeated twice. The responses to the first stimulation are shown in black, whereas those elicited by the second (applied 2 min after the first) are displayed in gray. The two horizontal lines indicate the zero-current level (*upper*) and the pre-stimulatory $[Ca^{2+}]_i$ (*lower*).

photorelease of caged Ca^{2+} elicits a bout of capacitance increase in excess of that produced by the train and that subsided 4 s after the flash of UV-light (arrow) although $[Ca^{2+}]_i$ remained ≥10 μM. The increases in cell capacitance evoked by the train and subsequent photorelease of caged Ca^{2+} (reaching an average $[Ca^{2+}]_i$ of 25 ± 5 μM) amounted to 341 ± 147 fF and 85 ± 17 fF. The cessation of exocytosis we interpret as the depletion of the RRP. Comparing the increase in cell capacitance elicited by the first 500-ms depolarization (49 ± 20 fF), which can be expected to fully deplete IRP (cf. Fig. 5 *B* and *C*) with the total increase in cell capacitance in response to the entire protocol (427 ± 141 fF) suggests that IRP only comprises ~10% of RRP. When the same stimulation protocol was applied 2 min later to allow $[Ca^{2+}]_i$ to return to basal and recovery of RRP, some interesting differences became evident. It can be observed that the Ca^{2+} currents are reduced by ≈30%, possibly a result of Ca^{2+}-dependent inactivation, and that the capacitance increase evoked by the second train of depolarizations is considerably smaller than those observed during the first train and averaged 163 ± 78 fF ($n = 5$; $p < 0.05$ vs. first train). However, exocytosis in response to photorelease of Ca^{2+} was more prominent and the total increase in cell capacitance produced by the entire protocol averaged 288 ± 103 fF (not statistically different from that

observed initially), suggesting that RRP had at least partially recovered.

Effects of intracellular Ca^{2+} buffering on exocytosis

If exocytosis is determined by the high $[Ca^{2+}]_i$ in the vicinity of the Ca^{2+} channels, then it should be unaffected by moderate elevation of the cytoplasmic Ca^{2+} buffering using Ca^{2+}-chelators such as EGTA (compare Adler et al., 1991). To assess the immediate effects of altered bulk cytosolic $[Ca^{2+}]$ and buffering capacity on exocytosis, we made use of the photosensitive Ca^{2+}-chelator diazo-2 (Fig. 6 *A*). After pre-loading with diazo-2, the cell was depolarized to zero mV for 500 ms. In a series of five experiments, resting $[Ca^{2+}]_i$ was determined as 0.18 ± 0.05 μM. The 500-ms depolarization increased $[Ca^{2+}]_i$ to 0.9 ± 0.3 μM and evoked a capacitance increase of 40 ± 12 fF. The cell was then allowed to recover for 2 min after which diazo-2 was activated by UV-irradiation. The release of diazo-2 reduced resting $[Ca^{2+}]_i$ to 0.09 ± 0.01 μM ($p < 0.01$) and a second depolarization applied 1 s after release of diazo-2 increased $[Ca^{2+}]_i$ to only 0.30 ± 0.05 μM. Nevertheless, the amplitude of the exocytotic response was unaffected and the capacitance increase still amounted to 40 ± 18 fF. The charge entry during the depolarization was the same before and after activation of diazo-2 and averaged 19 ± 5 pC in both instances. It is also apparent that endocytosis, seen as a decrease in cell capacitance, became less prominent after release of the Ca^{2+}-chelator. We have demonstrated elsewhere that endocytosis in B cells is Ca^{2+}-dependent (Eliasson et al., 1996), and the reduction of $[Ca^{2+}]_i$ may thus account for the slower endocytosis. This explanation requires that the Ca^{2+}-sensing of endocytosis is different from that of exocytosis, perhaps reflecting the global Ca^{2+} concentration rather than that just beneath the plasma membrane. Control experiments were performed to determine the influence of UV-irradiation on fura red fluorescence. It was then observed that at a free Ca^{2+} concentration of 0.1 μM, the fura red ratio increased by ≈20% after a flash of UV-light. Thus, it is possible that we underestimate the reduction of $[Ca^{2+}]_i$ resulting from photoactivation of diazo-2. If anything, exocytosis is therefore more resistant to Ca^{2+} buffering than suggested by the data of Fig. 6 *A*.

The failure of diazo-2 to affect exocytosis despite marked effects on resting and depolarization-evoked $[Ca^{2+}]_i$ again indicates that exocytosis is triggered by Ca^{2+} in close vicinity of the Ca^{2+} channel. We explored this aspect further by increasing cytosolic Ca^{2+} buffering by supplementing the pipette solution with 2 mM EGTA and 1 mM Ca^{2+} (estimated free Ca^{2+}: 0.23 μM). As shown in Fig. 6 *B*, a 500-ms voltage-clamp depolarization evoked a capacitance increase of 41 ± 8 fF ($n = 10$) when Ca^{2+} was strongly buffered, close to the 40 ± 12 fF obtained with no intracellular EGTA (see above). The integrated Ca^{2+} current

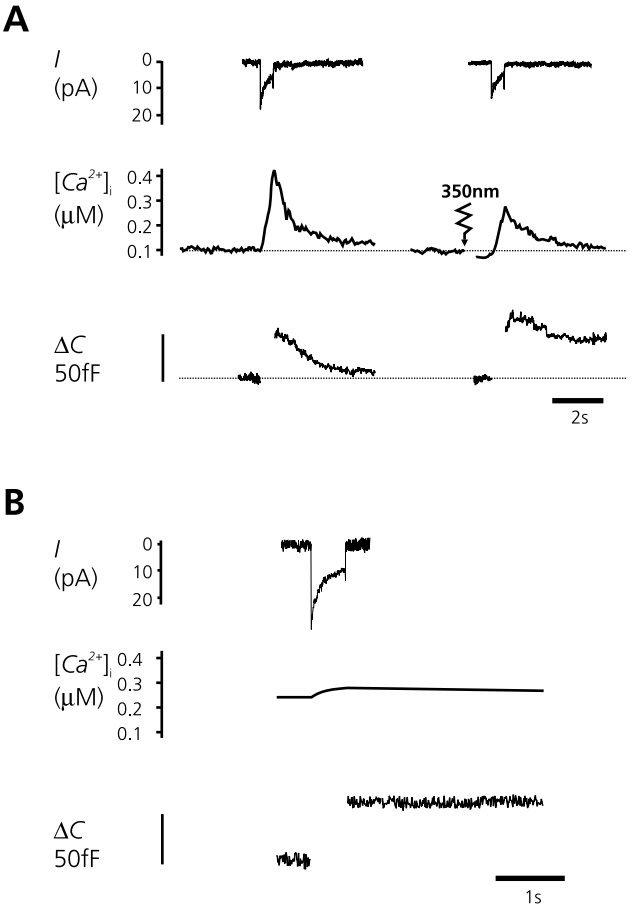

FIGURE 6 Regulation of exocytosis by submembrane and not global $[Ca^{2+}]_i$. (*A*) Ca^{2+} currents (*I*, *top*), $[Ca^{2+}]_i$ (*middle*), and membrane capacitance (ΔC, *bottom*) evoked in the same cell by two 500-ms depolarizations from −70 mV to 0 mV (indicated by steps above current trace) before (*left*) and after (*right*) photolytic release of the Ca^{2+} chelator diazo-2 (*arrow*). This compound changes its Ca^{2+} affinity from a K_d of 2.2 μM to 73 nM upon photolysis and was included at 0.3 mM in the pipette solution. Photolysis was initiated 1 s before the second depolarization. Note that exocytosis stops immediately after repolarization, although $[Ca^{2+}]_i$ remains elevated for several seconds and that it is unaffected by the release of diazo-2 despite reduction of basal and peak $[Ca^{2+}]_i$. (*B*) Ca^{2+} currents (*I*, *top*), exocytosis (ΔC, *bottom*), and calculated $[Ca^{2+}]_i$ evoked by a 500-ms depolarizations to zero when $[Ca^{2+}]_i$ was clamped at 0.23 μM with 2 mM EGTA and 1 mM Ca^{2+} ($[Ca^{2+}]_i$; *middle*). The change of $[Ca^{2+}]_i$ was estimated from the integrated Ca^{2+} current.

was 13 ± 3 pC, and we estimate that this amount of Ca^{2+} entry elevated $[Ca^{2+}]_i$ by only 35 nM.

Assembly of a functional complex between Ca^{2+} channels and secretory granules

We hypothesize that the rapid component of capacitance increase unveiled in Fig. 3 *B* and *C* reflects exocytosis of granules situated in the immediate vicinity of the voltage-gated Ca^{2+} channels in a way analogous to that documented for synaptic vesicles and N- and P-type Ca^{2+} channels in

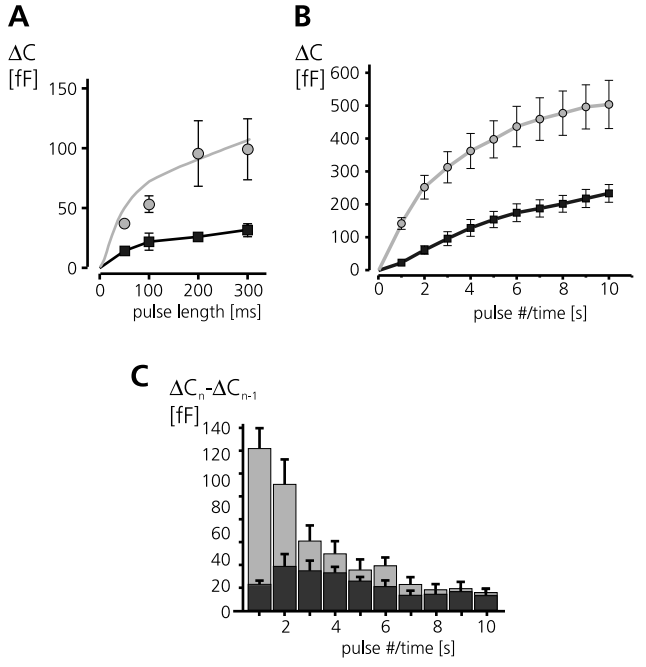

FIGURE 7 Physical interaction of Ca^{2+} channels with secretory granules is required for rapid, but not slow, exocytosis. (*A*) Increase in cell capacitance (ΔC) elicited by voltage-clamp depolarization lasting 50 to 300 ms from −70 mV to 0 mV under control conditions (○) and after supplementing the intracellular medium with 2.5 μM of $L_{c753-893}$ peptide of the $\alpha 1_C$ L-type Ca^{2+} channel (■). Data are presented as mean values of six (control, ●) and eight ($L_{C753-893}$) experiments. The curve superimposed on the data points is the same as in Fig. 3 *A*. The experiments were performed using the standard extracellular medium and pipette solution I. (*B*) Cumulative increase in cell capacitance (ΣC) during a train consisting of 10 500-ms depolarization to zero (stimulation frequency: 1 Hz) under control conditions (○) and after inclusion of the $L_{c753-893}$ (■) displayed against pulse number (= time). (*C*) As in *B* but the increment per pulse ($\Delta C_n - \Delta C_{n-1}$) during the train is shown for control (*light gray*) and $L_{C753-893}$ (*dark gray*).

the synapse (for review, see Catterall, 1999). Indeed, a recombinant protein corresponding to residues 753–893 of the $\alpha 1_C$ subunit of the L-type Ca^{2+} channel ($L_{c753-893}$), i.e., the part of the protein forming the loop connecting the second and the third homologous domains of the Ca^{2+} channel present in mouse B cells (Fig. 1), has the ability of associating with the exocytotic core complex proteins SNAP-25, syntaxin, and synaptotagmin (Wiser et al., 1999; Atlas, 2001). We have previously reported that intracellular application of $L_{c753-893}$ abolishes exocytosis evoked by single 500-ms depolarizations but is largely without effect on that elicited by photorelease of caged Ca^{2+} (Wiser et al., 1999). The selective effect of $L_{c753-893}$ on depolarization-evoked exocytosis suggests that the tethering of the Ca^{2+} channel to the secretory granules is functionally significant in the B cell and may account for the fast component of exocytosis. In Fig. 7 *A* we addressed this possibility by application of voltage-clamp depolarizations lasting 50 to 300 ms in the absence and presence of 2.5 μM of $L_{c753-893}$. Under control conditions, extending the duration of the depolarization evoked progressively larger exocytotic responses reaching a plateau of ≈100 fF within ≤300 ms (○). Consistent with the previous observations, inclusion of $L_{c753-893}$ strongly inhibited exocytosis at all times up to 350 ms (■) and the capacitance increase leveled off after an increase of ~20 fF. The fact that $L_{c753-893}$ had a weaker effect in this study than previously reported (Wiser et al., 1999), we attribute to the use of a somewhat lower concentration of the peptide in this study (2.5 μM instead of 10 μM).

We next tested the effects of $L_{C753-893}$ when exocytosis was elicited by a train of ten 500-ms depolarization applied at 1 Hz (Fig. 7 *B*). As expected, the response to the first depolarization was much reduced. However, subsequent stimuli evoked capacitance increases that were comparable with those observed under control conditions. This becomes obvious when the net increase per pulse is plotted (Fig. 7 *C*). Under control conditions (light gray), the secretory response is clearly biphasic: the two first depolarization evoke capacitance increases >100 fF, whereas the responses to subsequent depolarizations settled at a steady level of ~20 fF capacitance increase per pulse. In the presence of the $L_{c753-893}$ (dark gray), the capacitance increases evoked by a single depolarization varied between 20 and 40 fF throughout the train.

Influence of Ca^{2+} channel gating on exocytosis

If exocytosis were determined by the activity of single Ca^{2+} channels, then experimental maneuvers that affect the Ca^{2+} channel mean open time (τ_{open}) should influence secretion. The Ca^{2+} channel agonist BayK8644 (1 μM) increases τ_{open} from 1.9 ± 0.3 ms under control conditions (Fig. 8 *A*) to 11.7 ± 1.6 ms (Fig. 8 *B*). The mean closed times (τ_{closed}) were determined, from records that contained only a single active channel, as 63 ± 20 ms under control conditions and 52 ± 29 ms in the presence of BayK8644. These effects on the single-channel kinetics correlated with a 30% increase in the peak whole-cell Ca^{2+} current (from a basal amplitude of 120 ± 7 pA to 162 ± 5 in the presence of the agonist; $p < 0.01$) and a 30% increase in the integrated Ca^{2+} current for depolarizations ≤100 ms (Fig. 8 *C*). Figure 8 *D* summarizes the relationship between pulse duration and exocytosis evoked by 5- to 350-ms depolarizations in the absence (○) and presence of 1 μM BayK8644 (●). Bay K8644 increased the exocytotic responses elicited by the 15- and 30-ms depolarizations but had no statistically significant effect at the longer depolarizations. When exocytosis (ΔC) is plotted as a function of Ca^{2+} entry (Q), it becomes clear that the relationships are linear for integrated Ca^{2+} currents <5 pC (corresponding to depolarizations ≤150 ms; Fig. 8 *E*) and that the data points recorded in the absence and presence of the agonist largely superimpose. The slope of the indicated line (drawn by eye) corresponds to 18 fF capacitance increase per pC Ca^{2+} entry. We conclude that

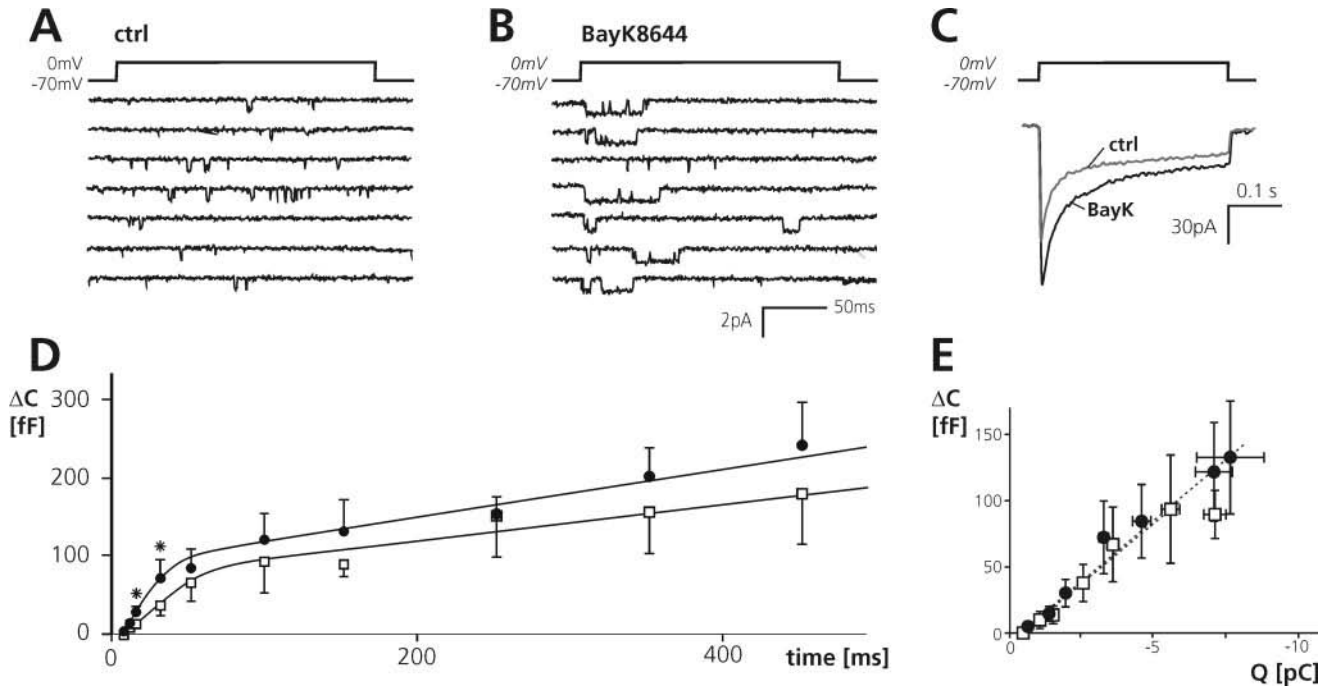

FIGURE 8 Prolonged Ca^{2+} channel mean open time does not enhance exocytosis. Recordings of single Ca^{2+} channels in cell-attached patches in the absence (*A*) and presence (*B*) of 1 μM BayK8644 with 110 mM Ba^{2+} as charge carrier. (*C*) Whole-cell Ca^{2+} currents evoked by a 500-ms depolarization from −70 mV to 0 mV recorded at 2.6 mM extracellular Ca^{2+} in the absence (ctrl) and presence of 1 μM BayK8644 (BayK). (*D*) Relationship between pulse duration and increases in cell capacitance (ΔC) elicited by voltage-clamp depolarization from −70 mV to 0 mV lasting 5 to 450 ms under control conditions (□) and after supplementing the extracellular medium with 1 μM BayK8644 (●). The curves were obtained by fitting Eq. 5 to the data points. *$p < 0.05$. (*E*) Relationship between integrated Ca^{2+} current (Q) and exocytotic response (ΔC) under control conditions (□) and in the presence of Bay K8644 (●). The straight line is drawn by eye. In *D* and *E*, the data are presented as mean ± SE of six experiments. Experiments in *C–E* were carried out using perforated patch whole-cell recording mode.

the effects of Bay K8644 on exocytosis elicited by brief depolarizations can be explained entirely by the larger Ca^{2+} currents and that prolonging the Ca^{2+} channel mean open time only marginally influences exocytosis.

In a second series of experiments the peak Ca^{2+} current was instead increased by elevating the extracellular Ca^{2+} concentration to 10 mM. This enhances Ca^{2+} influx by an increased driving force rather than changes of channel gating and kinetics. The peak Ca^{2+} current increased from 120 ± 7 pA at 2.6 mM extracellular Ca^{2+} to 162 ± 14 pA ($p < 0.01$) at 10 mM Ca^{2+} (Fig. 9 *A*). The exocytotic response elicited by a 15-ms depolarization (i.e., before completion of Ca^{2+} current inactivation) increased from a control value of 13 ± 7 fF ($n = 6$) to 48 ± 2 fF ($n = 4$; $p < 0.005$) at high Ca^{2+}. However, increasing Ca^{2+} also accelerated Ca^{2+} current inactivation, and the integrated Ca^{2+} current was actually reduced for all depolarizations ≥30 ms. Accordingly, the amplitude of the exocytotic responses elicited by depolarizations ≥250 ms was smaller in the presence of high extracellular Ca^{2+} (▲) than the control responses (□; Fig. 9 *C*). We acknowledge that as a consequence of increased concomitant Ca^{2+}-dependent endocytosis (Eliasson et al., 1996) the observed values of capacitance increase may underestimate exocytosis and thus account for the paradoxical reduction at depolarizations lasting ≥250 ms. Fig. 9 C summarizes the relationship between the integrated Ca^{2+} current and the exocytotic responses elicited by depolarizations lasting 5 to 250 ms. Again the data can be described by straight lines for integrated Ca^{2+} currents ≤5 pC (i.e., depolarizations < 150 ms), but the relationship is steeper in the presence of high extracellular Ca^{2+} than what was observed under control conditions (30 fF/pC vs. 18 fF/pC).

Evidence for Ca^{2+} channel clustering

The failure of BayK8644 to exert any marked effects on exocytosis despite a sixfold increase in the mean lifetime may suggest that several Ca^{2+} channels cooperate to produce the $[Ca^{2+}]_i$-transient regulating exocytosis. To determine whether Ca^{2+} channels are evenly distributed or rather form functional complexes of several channels we analyzed recordings of unitary Ca^{2+} channel activity in 22 consecutive cell-attached patch recordings in which channel activity had been maximized by the presence of BayK8644 (Fig. 10 *A*). The frequency histogram of the number of active channels per patch is shown in Fig. 10 *B*. More than 60% of the

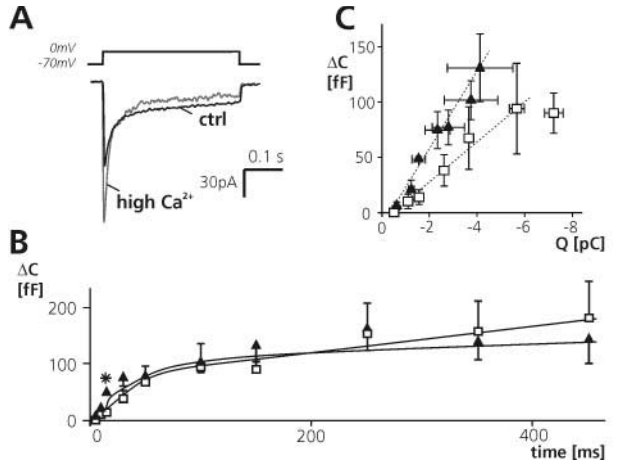

FIGURE 9 Elevation of extracellular Ca^{2+} stimulates exocytosis elicited by short depolarizations. (*A*) Whole-cell Ca^{2+} currents evoked by a 500-ms depolarization from −70 mV to 0 mV recorded at 2.6 mM (ctrl) and 10 mM (high Ca^{2+}) extracellular Ca^{2+}. (*B*) Relationship between pulse duration and increases in cell capacitance (ΔC) elicited by voltage-clamp depolarization from −70 mV to 0 mV lasting 5 to 450 ms under control conditions (□) and after increasing extracellular Ca^{2+} concentration to 10 mM (▲). The superimposed curves were obtained by approximating Eq. 5 to the data points. (*C*) Relationship between integrated Ca^{2+} current (Q) and exocytotic response (ΔC) under control conditions (□) and after elevation of extracellular Ca^{2+} (▲). The straight lines were drawn by eye. Data in *B* and *C* are mean ± SE of six (control, same as in Fig. 8) and four (high Ca^{2+}) experiments. $*p < 0.01$. Experiments were performed using the perforated patch whole-cell technique.

patches contained no active channels. Ca^{2+} channel openings were seen in a total of seven patches of which four contained three simultaneously active channels.

DISCUSSION

How can a cell secrete at high speed in an accurate and robust fashion with few Ca^{2+} channels? This is the problem faced by the insulin-producing B cell, a cell equipped with fewer than 500 Ca^{2+} channels and yet capable of Ca^{2+}-dependent exocytosis at a rate approaching 650 granules/s. We propose that the B cell achieves this by tethering the Ca^{2+} channels to the secretory granules so that the secretory machinery is exposed to exocytotic levels of Ca^{2+} (≥10 μM) upon Ca^{2+} channel opening. Here we discuss the functional consequences and advantages of this arrangement.

The B cell contains <500 $\alpha 1_C$ L-type Ca^{2+} channels

The largest Ca^{2+} current in the B cell is observed during depolarizations to 0 mV where it reaches a peak amplitude of ≈80 pA when measured at 2.6 mM extracellular Ca^{2+}. The B cell Ca^{2+} current is sensitive to nifedipine and BayK8644 (Rorsman and Trube, 1986; Rorsman et al., 1988) but resistant to ω-conotoxin MVIIC, ω-agatoxin IVA, and ω-conotoxin GVIA (Gilon et al., 1997). These data suggest that in mouse B cells, the Ca^{2+} current principally flows through L-type Ca^{2+} channels and that N-, P-, and Q-type Ca^{2+} channels do not measurably (if at all) contribute to the influx of the ion.

L-type Ca^{2+} channels are composed of either $\alpha 1_C$- or $\alpha 1_D$-subunits (Striessnig et al., 1998). Analysis of the mRNAs encoding the α_1-subunit suggests that the B cell Ca^{2+} channel contains the α_{1D}-subunit (Seino et al., 1992) and expression of this subunit in B cells from obese hyperglycemic (*ob*/*ob*) mice has indeed been verified by Western-blot analysis (Yang et al., 1999). Using the same antibody, we failed to detect expression of $\alpha 1_D$ in NMRI mouse B cells, whereas $\alpha 1_C$ was readily detected (Fig. 1 *D*). We did, however, detect $\alpha 1_D$ mRNA in islets from these mice, but it seems likely that this reflects expression in non-B cells, because some non-B cells in the islet preparation were stained with the $\alpha 1_D$ antibody. The idea that α_{1D} Ca^{2+} channels do not contribute significantly to the B cell whole-cell Ca^{2+} current is reinforced by experiments on B cells isolated from $\alpha 1_D$ knockout mice (Platzer et al., 2000), and we demonstrate here that genetic ablation of $\alpha 1_D$- Ca^{2+} channels neither affects the voltage dependence, nor the amplitude of the B cell Ca^{2+} current (Fig. 1 *B*). Although we cannot exclude that compensatory up-regulation of $\alpha 1_C$ takes place in the knockout mice, the latter results taken together with the immunofluorescence microscopy argue that the L-type Ca^{2+} channel of mouse B cell consists predominantly, if not exclusively, of $\alpha 1_C$ Ca^{2+} channels.

The Ca^{2+} channel density of the B cell was estimated to be 450 channels per cell (Fig. 2). Surprisingly, this important functional parameter has not been determined previously and efforts to model the sub-membrane $[Ca^{2+}]_i$ in the B cell (Gil et al., 2000) have been based on the same Ca^{2+} channel density as in other endocrine cells. The value of 0.9 channels/μm^2 we report here for the B cell is only 5 to 10% of those reported for adrenal chromaffin cells (9–20 channels/μm^2; Fenwick et al., 1982; Klingauf and Neher, 1997) or retinal bipolar cells (15 channels/μm^2; von Gersdorff et al., 1998) and corresponds to a mean distance between two Ca^{2+} channels of 1.2 μm. The low Ca^{2+} channel density in the B cell taken together with the finding that exocytosis operates at $[Ca^{2+}]_i$ as high as 30 μM (Fig. 4) have important functional implications. With so few Ca^{2+} channels, $[Ca^{2+}]_i$ will rise to exocytotic levels only in the immediate vicinity of the Ca^{2+} channels. Indeed, the finding that increasing Ca^{2+} influx by elevation of extracellular Ca^{2+} produces a strong (>3.5-fold) enhancement of exocytosis elicited by short (≤15 ms) depolarizations, which is too short for $[Ca^{2+}]_i$ to equilibrate, supports the idea that the Ca^{2+}-sensor for exocytosis is situated close to the inner mouth of the Ca^{2+} channel(s).

We have previously reported that Ca^{2+} entry in the B cell (active Ca^{2+} channels or localized increases in $[Ca^{2+}]_i$) is

polarized to the part of the cell containing the highest granule density (Bokvist et al., 1995). Such a polarity is not so evident in the immunostaining presented in Fig. 1 *E*, but this is not necessarily in conflict with the previous results. It has been suggested that syntaxin acts as a scaffold for the exocytotic machinery keeping the proteins of the granule docking site in place and controlling the activity of the Ca^{2+} channels depending on whether the release site is occupied by a vesicle or not (Wu et al., 1999). Interestingly, syntaxin alone (i.e., in the absence of other synaptic proteins) binds to N-type Ca^{2+} channels and thereby decreases its activity (Bezprozvanny et al., 1995) and it exerts the same effect on $\alpha 1_C$ L-type Ca^{2+} channels, the type present in mouse B cells (Wiser et al., 1999). Thus, the failure to observe functional Ca^{2+} channels during single-channel recordings or increases in $[Ca^{2+}]_i$ in the part of the B cell devoid of granules (Bokvist et al., 1995) should not be interpreted in terms of the channel protein being absent. Rather, it is possible that the channel protein is in an inactive state, which is still detectable by immunostaining.

Exocytosis is not determined by Ca^{2+} influx through individual Ca^{2+} channels but rather complexes of several channels

Under control conditions, the mean open time (τ_{open}) of the Ca^{2+} channel during a depolarization to zero mV was ≈2 ms (Fig. 8 *A*). In experiments involving photorelease of caged Ca^{2+} the delay between elevation of $[Ca^{2+}]_i$ and the initiation of exocytosis (t_{lat}) was 10 ± 3 ms (Fig. 4 *B*), which is approximately threefold longer than the time required for the Ca^{2+} current to reach the peak amplitude. Assuming that t_{lat} is the minimum period $[Ca^{2+}]_i$ needs to be elevated to evoke exocytosis and that the time needed for Ca^{2+} channel activation is negligible, only 0.5% of the Ca^{2+} channel openings are long enough to result in exocytosis (i.e., $100 \times \exp[-t_{lat}/\tau_o]$). This argues that Ca^{2+} channel clustering would be functionally advantageous. For example, if we assume (for reasons that will become evident below) that the Ca^{2+} channels exist in triplets, then the chance that at least one of the channels is open long enough during the depolarization to trigger exocytosis increases at least threefold. We have modeled this situation and thereby taken into account that one long opening can be substituted for by several overlapping openings of shorter duration. For the mean open and shut times of the channel reported here, the chances that $[Ca^{2+}]_i$ is present at exocytotic levels sufficiently long during 50 ms increases to 18.6% with a triplet of Ca^{2+} channels forming a complex with a granule (see Appendix 1 and dotted lines in Fig. 10 *D*).

Indirect support of the idea that Ca^{2+} channel clustering is important can also be derived from the marginal effects of the Ca^{2+} channel agonist BayK8644 on exocytosis (Fig. 8). If exocytosis were controlled by $[Ca^{2+}]_i$ in the vicinity of single Ca^{2+} channels, then the Ca^{2+} channel agonist should be expected to have a strong effect on exocytosis as it increases τ_o to 12 ms. In the presence of BayK8644, >40% of the openings are long enough to evoke exocytosis. However, only a slight twofold stimulation of exocytosis by Bay K8644 was observed (Fig. 8 *D*). The latter effect is in fact weaker than the enhancement obtained when Ca^{2+} entry was instead accelerated by an increased driving force (Fig. 9 *B*). Collectively these findings suggest that 1) Ca^{2+} channel activity during membrane depolarization nearly saturates the Ca^{2+}-sensor already under control conditions (Gil et al., 2000) and 2) although exocytosis is regulated by $[Ca^{2+}]_i$ in the vicinity of the Ca^{2+} channels, it is not determined by Ca^{2+} influx through individual Ca^{2+} channels. Given these data it seems more likely that several Ca^{2+} channels cooperate to produce the $[Ca^{2+}]_i$-transient that regulates exocytosis. Such an arrangement would increase the robustness of the secretory machinery and cancel out the influence of stochastic variations of Ca^{2+} channel activity on exocytosis.

Estimation of the Ca^{2+} channel: granule stoichiometry

Comparison of the number of Ca^{2+} channels per B cell (450; Fig. 2) with the number of docked granules per B cell (≈600; Olofsson, Göpel, Barg, Galvanovskis, Ma, Salehi, Rorsman, and Eliasson, manuscript submitted) suggests that the Ca^{2+} channels and granules associate with a stoichiometry of <1 Ca^{2+} channel per secretory granule. This is only 15 to 20% of the corresponding value in retinal bipolar neurons (5–7 functional channels per docked vesicle; von Gersdorff et al., 1998). However, it is clear from the kinetic analysis of depolarization-evoked exocytosis (Fig. 3) that only 60 granules of the granules closely associate with the Ca^{2+} channels (i.e., IRP; Voets et al., 1999). An upper estimate of the Ca^{2+} channels per IRP granule stoichiometry is therefore ≈7:1.

Single-channel recordings were applied to determine whether Ca^{2+} channels are clustered (Fig. 10). Somewhat surprisingly, close to 20% of the patches contained three active channels. Our pipettes were pulled from borosilicate glass and had a tip resistance of 2 MΩ. From this value we can estimate that the pipette tip diameter is ≈1 μm (Sakmann and Neher, 1995). The probability of finding a certain number of channels in a patch of this size assuming random distribution is shown by the dotted line superimposed on the histogram in Fig. 10 *B* and *C*. With 450 channels in the cell, the likelihood is greatest of finding either a single channel or no channels at all in the patch. A narrower patch ($d = 0.5$ μm) results in a steeper distribution with 80% of the patches lacking channel activity and virtually no patches containing two or more active channels (Fig. 10 *C*, dashed line). Increasing the patch diameter skews and broadens the distribution. For example, with a pipette diameter of 1.5 μm,

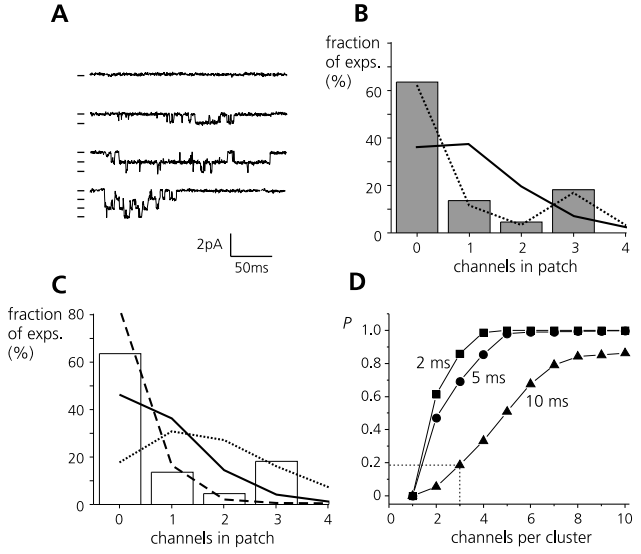

FIGURE 10 B cell Ca^{2+} channels are not uniformly distributed. (*A*) Typical recordings of unitary Ca^{2+} channel activity recorded in the cell-attached mode from four different cells with 110 mM Ba^{2+} as charge carrier. (*B*) Distribution of the observed maximum number of open levels observed in 22 consecutive patches. The curves show the calculated distribution assuming 450 randomly placed single Ca^{2+} channels (*continuous line*) and the best fit (see Appendix 2) to the experimental data with 80 single channels, 14 doublets, 114 triplets, and no greater order clusters of Ca^{2+} channels (*dotted line*). In both cases, the patch diameter was taken to be 1.15 μm. (*C*) Calculated distributions assuming 450 randomly placed single channels and pipette diameters of 0.5 μm (*dashed line*), 1 μm (*continuous line*), or 1.5 μm (*dotted line*). (*D*) Calculated probabilities (see Appendix 1) for single and overlapping channel openings exceeding t_{lat} = 10 ms (▲), t_{lat} = 5 ms (●), and t_{lat} = 2 ms (■) during a 50-ms depolarization.

17% of the patches will contain zero channels, 31% one channel, 27% two channels, and 25% three or more channels (Fig. 10 *C*, dotted line). It is clear that none of these distributions describes that observed experimentally (rectangles), and we conclude therefore that the Ca^{2+} channels in the B cell are not randomly distributed. We have made a theoretical evaluation of the experimental distribution, and this analysis leads us to propose that the B cell contains ~115 calcium channel triplets (see Appendix 2). We speculate that each of these triplets associate with individual secretory granules and thus form an "exocytotic complex." Comparison of our value of IRP (≈60 granules/cell) with the number of Ca^{2+} channel triplets suggests that there is an approximate twofold excess of Ca^{2+} channel clusters. It is possible that the superfluous clusters represent channels that have associated with unprimed granules that are not yet release competent.

Functional importance of rapid exocytosis

We demonstrate that a subset of 60 granules in the B cell can be released at a very high rate (>600 granules/s) in a surprisingly short period (50–100 ms; Fig. 3 *B*) and with minimal latency (≤15 ms). The latter value is similar to that observed upon release of caged Ca^{2+} (10 ms; Fig. 4 *B*), suggesting that diffusion of Ca^{2+} in the cytosol is not rate-limiting to exocytosis and that the delay is an inherent property of the exocytotic machinery. As discussed above, we believe that the ultrafast component arises as a consequence of a close association between the secretory granules and triplets of Ca^{2+} channels. It seems unlikely that speed is the prime objective because insulin acts systemically once released into the blood stream. Rather, the arrangement is likely to be a consequence of the few Ca^{2+} channels present in the B cell. With a Ca^{2+} channel density as low as 0.9 channels/μm^2, it is essential that the Ca^{2+} actually entering the cells is made use of in the most efficient way. This is accomplished if the secretory granules and Ca^{2+} channels assemble into a functional complex. The short delay between membrane depolarization and exocytosis is a by-effect of, but not the reason for, this arrangement. It seems possible that efficient usage of Ca^{2+} is a functional adaptation of the B cell, whereby it allows large exocytotic responses during protracted periods while minimizing the expenditure of metabolic energy required to restore the cytosolic Ca^{2+} concentration. Ca^{2+}-pumping by the Ca^{2+}-ATPases in the plasma membrane and in the endoplasmic reticulum is significant in this context (Gall et al., 1999) with resultant lowering of the cytoplasmic ATP:ADP-ratio (Detimary et al., 1998). This is obviously an undesirable effect in a cell that uses ATP-regulated K^+ channels to couple an increase in the blood glucose to stimulated secretion of insulin (for review, see Ashcroft and Gribble, 1999).

Exocytosis operates at high $[Ca^{2+}]_i$

Our data confirm previous observations (Takahashi et al., 1997) that exocytosis is regulated by Ca^{2+} with a K_d as high as ≈20 μM. In a cell with as few Ca^{2+} channels as the B cell, such high concentration is attained only in the close vicinity of the Ca^{2+} channels. The data obtained with $L_{c753-893}$ indicates that the (triplets of) Ca^{2+} channels are tethered to the granules by the cytoplasmic loop of the L-type Ca^{2+} channel protein. This implies that exocytosis operates at close to saturating $[Ca^{2+}]_i$ and that the zone where this occurs is confined to the vicinity of the Ca^{2+} channel(s) and the period of channel opening. Assuming an α-helical arrangement, each amino acid corresponds to 0.15 nm, and we can estimate that the total length of $L_{c753-893}$ is ≈20 nm and the maximum distance between the Ca^{2+} channel and the granule 10 nm (20/2 nm because the loop has to extend both ways). Inclusion of $L_{c753-893}$ in the intracellular solution appears to selectively prevent exocytosis of granules belonging to IRP, and this pool may therefore correspond to granules that have associated with the Ca^{2+} channels. This pool is quickly (≤300 ms) depleted during depolarization. At later times and during repetitive (1

Hz) stimulation, $[Ca^{2+}]_i$ may rise sufficiently throughout the cell to trigger exocytosis of RRP granules that have not associated with the Ca^{2+} channels, and this accounts for the component of exocytosis that is insensitive to exogenous $L_{c753-893}$ (Fig. 7 *B* and *C*).

The close proximity of the Ca^{2+} channels and the secretory granules is probably the explanation to the observations that exocytosis normally echoes Ca^{2+} channel activation (Ämmälä et al., 1993; Bokvist et al., 1995; Eliasson et al., 1996; Renström et al., 1996) and stops immediately when the membrane potential is stepped back to the holding potential. Regulation of exocytosis by Ca^{2+} in the close vicinity of the Ca^{2+} channels is in keeping with the finding that addition of EGTA is without inhibitory action on exocytosis when supplied with Ca^{2+} at a 2:1 ratio (2 mM EGTA and 1 mM Ca^{2+}). The previous observation that EGTA is a strong inhibitor of exocytosis when added without Ca^{2+} (Ämmälä et al., 1993) suggests that subexocytotic concentration of Ca^{2+} is required to maintain the size of IRP and/or prevent depriming of the secretory granules (Gromada et al., 1999).

By analogy with the situation in chromaffin cells, IRP represents a subset of the RRP also in the B cell. Comparing the magnitude of the exocytotic response that can be elicited by a 500-ms depolarization (which likely leads to complete depletion of IRP as suggested by kinetic analysis in Fig. 3 *C*) with the capacitance increase that is evoked by subsequent photoliberation of caged Ca^{2+} suggests that IRP comprises ~10% of RRP, similar to the value reported for chromaffin cells. The number of RRP granules is likewise not so different between the two cell types; 140 in chromaffin cells and ≈300 in B cells in the presence of cAMP, which increases RRP four- to sevenfold (Renström et al., 1996). The special feature of the B cell is that high-speed exocytosis (1.1 pF/s or 640 granules/s) is initiated with a short delay (≥10 ms in experiments involving photorelease of caged Ca^{2+} and < 15 ms when the cells were stimulated by voltage-clamp depolarizations; Figs. 3 *B* and 4 *B*) with a Ca^{2+} channel density only 5 to 10% of that seen in the chromaffin cells. As discussed above, the efficient usage of Ca^{2+}-entering the cell may be achieved by tethering the Ca^{2+} channels to the secretory granules (IRP).

It is interesting to compare the recovery of RRP and IRP in the experiments combining voltage-clamp depolarization and photorelease of caged Ca^{2+} (Fig. 5). Whereas RRP recovers completely during a 2-min interval, as evidenced by the same amplitude of the total exocytotic response being elicited by the first and second stimulation sequences, exocytosis elicited by the voltage-clamp depolarizations, principally reflecting release of IRP, was much reduced during the second round of stimulation. Apparently, replenishment of IRP requires a longer time and/or additional processes to be completed than does the recovery of RRP. Conceivably, refilling of IRP involves the physical movement of either the secretory granules or the Ca^{2+} channels so that new Ca^{2+} channel/granule-complexes, capable of rapid exocytosis, can be formed. It is pertinent that exocytosis during the second stimulation is similar to that observed in the presence of $L_{c753-893}$ (compare Figs. 5 and 7C); almost no capacitance increase during the first depolarization and small capacitance steps (~20 fF) being elicited by the subsequent pulses. In this context it may finally be of relevance that granule movements (visualized using enhanced green fluorescent protein tagged to the granule protein islet amyloid polypeptide) cease within a few minutes after establishment of the whole-cell configuration (S. Barg, unpublished observations).

Physiological and pathophysiological implications

Glucose-stimulated insulin secretion in vivo typically follows a biphasic time course consisting of a transient (10-min duration) first phase followed by a sustained second phase. We have estimated that the number of granules released during first-phase insulin secretion totals 50 to 100 granules per B cell (Rorsman et al., 2000). This value is obviously not too different from the 60 granules that undergo exocytosis within the first 200 ms of a depolarization (Fig. 3 *B*), and it seems reasonable to conclude that these granules account for first phase insulin secretion. Type-2 diabetes is associated with the loss of first phase insulin secretion, whereas second phase release is less affected (for review, see Cerasi, 1992). The finding that inclusion of $L_{c753-893}$ in the intracellular solution leads to the selective abolition of an early component of release with little effect on slow exocytosis finally raises the interesting possibility that failure of the insulin-containing secretory granules to correctly associate with the L-type Ca^{2+} channels in the B cell contributes to the secretion defect seen in diabetes. It is therefore of great interest that diabetic GK-rats exhibit decreased expression of the t-SNARE proteins syntaxin and SNAP-25, to which $Lc_{753-893}$ binds, and that experimental procedures that normalize the levels of these proteins result in improved glucose responsiveness (Nagamatsu et al., 1999).

APPENDIX

1. Effect of Ca^{2+} channel clustering on the probability of exocytosis

Our data suggest that exocytosis of a granule occurs at intracellular Ca^{2+} concentrations that nearly saturate the Ca^{2+}-sensor of exocytosis (>25 μM). Such conditions should be limited to the immediate vicinity of the pore of the open channel. We assume in this context a "waiting" time period t_{lat}, during which Ca^{2+} needs to be present at such high concentrations for exocytosis to be triggered. This is suggested by the delays in the order of a few milliseconds upon flash release of caged Ca^{2+} (Fig. 4 *B*). The necessary increase in Ca^{2+} concentration can be achieved by one or several Ca^{2+} channels (with open and shut times m_o and m_s) in the vicinity of the granule that stay open during t_{lat}. The probability of a secretory granule undergoing exocytosis equals the probability that the "waiting"

time for at least one channel to be continuously open during t_{lat}. Long openings of single channels can be substituted with overlapping openings of several channels, each of the openings having a duration $<t_{lat}$. To investigate the effect of channel clustering on this probability, we carried out numerical simulations on a system of identical two-state channels. A set of dwell times in shut and open states was generated with the help of a source equation

$$\frac{\tau_k}{\tau} = -\ln(RND) \qquad \text{(A1.1)}$$

in which τ is equal to m_0 (1.9 ms) or m_s (5 ms), τ_k ($k = 1, 2, 3\ldots, n$) is a consecutive dwell time in a given state, and *RND* is a random number chosen uniformly inside the interval 0 to 1. All channels were assumed to be in the closed state at the beginning of the simulation process. Every individual simulation process was run until the event "at least one channel is open during t_{lat}" occurred. This process was repeated 400 times, and the collected data were used to create the distribution histograms for waiting times in clusters consisting of a variable number of channels. The probability distribution functions for waiting times were then estimated by fitting the gamma distribution to the simulated waiting time frequency histograms (data not shown), and the fraction of events $>t_{lat}$ during the depolarization was obtained by integrating the probability distribution functions. A theoretical treatment of this problem is in preparation (Galvanovskis and Söderberg, manuscript in preparation).

2. Distribution function for the number of channels per patch

Consider a spherical cell having a diameter D and a patch of diameter d_{patch}. Single channels and clusters are randomly and independently distributed and their area negligible. It is assumed that the presence of a channel or a cluster of channels in a patch does not affect the probability for other channels to be found in it. Because a channel or cluster can only be inside or outside the patch, the distribution function for a random variable $S(k_1, k_2, \ldots, k_i)$ reflecting the number of the various objects in the patch will be the product of binomial distributions for every object class present is given by the expression

$$p_{k_1,k_2,k_3\ldots k_i} = C_{n_1}^{k_1} C_{n_2}^{k_2} C_{n_3}^{k_3} \cdots C_{n_i}^{k_i} p^{k_1+k_2+k_3+\cdots k_i} \times (1-p)^{N-k_1-k_2-k_3-\cdots-k_i} \qquad \text{(A2.1)}$$

in which $n_1, n_2, n_3, \ldots, n_i$ are the numbers of single channels, doublets, and so forth, found in a patch, N is the total number of objects in a patch, and $C_{n_i}^{k_i}$ are binomial coefficients; $p_{k_1,k_2,\cdots k_i}$ is the probability that the patch membrane contains k_1 single channels, k_2 doublets, k_3 triplets, and so on. Here the parameter p is the probability for a single object, a single channel, a doublet, a triplet, and so on, to be found in a patch and is defined as a ratio of the patch area to the total area of cell surface

$$p = \frac{\text{patch area}}{\text{area of cell surface}} = \frac{d_{patch}}{4D} \qquad \text{(A2.2)}$$

However, a patch-clamp experiment does not allow one to observe directly the random variable $S(k_1, k_2, \ldots, k_i)$ because the openings of an individual channel or a channel within a cluster are indistinguishable events. Under certain conditions (see later in this Appendix), the observable random variable S_s is the total number of channels s, single as well as clustered, in a patch membrane. To compare experimental data on channel distribution in a patch membrane with theoretical expectations, the distribution function of S_s should be derived. This can be done by recognizing that any event from the sample space of S_s "s channels have been observed in a patch" actually consists of a series of experimentally identical subevents from the sample space of $S(k_1, k_2, \ldots, k_i)$. Each of these subevents leads to the inclusion in a patch of s channels and is realized by different arrangements of single channels and clusters of various numbers of channels in a patch. The total number and composition of these subevents is found by solving in integers the linear equation

$$x_1 + 2x_2 + 3x_3 + \cdots + ix_i = s \qquad \text{(A2.3)}$$

in which $x_1, x_2, x_3, \ldots x_i$ is the number of corresponding objects included in a patch. Finally, the probability of the event "s channels observed" and the sought distribution function of the random variable S_s are equal to the sum of probabilities of all subevents comprising this event

$$p(s \text{ channels observed}) = \sum_j p_{x_1^j x_2^j \ldots x_i^j}. \qquad \text{(A2.4)}$$

A program was written in MATLAB that solved in integers Eq. A2.3 and allowed splitting all imaginable events from the sample space of S_s into series of subevents from $S(k_1, k_2, \ldots, k_i)$. Further, it found the distribution function for S_s with the help of Eq. A2.1. To determine the character of channel clustering in B cells, this function was then fit to channel distribution data obtained in patch-clamp measurements (Fig. 10). To this end it was assumed that the cell surface contains single channels and clusters of two, three, four, five, and six channels. Fitting parameters were the corresponding numbers n_1, n_2, n_3, n_4, and n_5 of these objects and the diameter of the patch. The inclusion of clusters of higher order was not necessary because their corresponding probabilities were practically zero.

3. Probability for all channels in a patch to open simultaneously

The approach used above to derive the channel distribution function rests on the assumption that the number of channels in a patch membrane can be detected by the analysis of channel current recordings. More specifically, it is assumed that the maximum number of channel superimpositions reflects the true number of channels in the patch. The following considerations suggest this is an acceptable approximation. Consider k identical channels within the same patch of membrane. Let m_o and m_s be the open and shut times of this type of a channel. The probability of finding a channel open at any time t is

$$p_{open} = \frac{m_{open}}{m_{open} + m_{shut}}. \qquad \text{(A3.1)}$$

The probability of all k channels being open simultaneously at any time t is then

$$p_{open}^k = \left(\frac{m_{open}}{m_{open} + m_{shut}}\right)^k \qquad \text{(A3.2)}$$

For $m_o = 12$ ms and $m_s = 5$ ms, and two channels in a patch p is 0.09. In a recording lasting a total of 50×200 ms (as is typical for our experiments) and a sampling period of 0.1 ms, it is reasonable to assume that all channels are simultaneously open at least once during the experiment. It should therefore be valid to use the maximum number of observed superimpositions as the number of channels actually present in the patch membrane.

We thank Kristina Borglid for expert technical assistance.

This work was supported by the Swedish Medical Research Council (grant nos. 8647, 12234, 13147, and 13509), the Swedish Diabetes Association, the European Commission (HPRN-CT-2000-00082), the Juvenile Diabetes Research Foundation, the Knut and Alice Wallenberg Foundation, the Novo Nordisk Foundation, the Segerfalkska Stiftelsen, the Crafoordstiftelsen, the National Agency for Planning and Coordination of Research (FRN), the Aage and Louise Hansen Foundation. Erik Renström was

supported by the Amylin Paul Langerhans Award of the European Association for the Study of Diabetes, and Stiftelsen för vetenskapligt arbete inom diabetologin.

REFERENCES

Adler, E. M., G. J. Augustine, S. N. Duffy, and M. P. Charlton. 1991. Alien intracellular calcium chelators attenuate neurotransmitter release at the squid giant synapse. *J. Neurosci.* 11:1496–1507.

Ämmälä, C., L. Eliasson, K. Bokvist, O. Larsson, F. M. Ashcroft, and P. Rorsman. 1993. Exocytosis elicited by action potentials and voltage-clamp calcium currents in individual mouse pancreatic B-cells. *J. Physiol.* 474:665–688.

Ashcroft, F. M., and F. M. Gribble. 1999. ATP-sensitive K^+ channels and insulin secretion: their role in health and disease. *Diabetologia.* 42: 903–919.

Ashcroft, F. M., and P. Rorsman. 1989. Electrophysiology of the pancreatic β-cell. *Prog. Biophys. Molec. Biol.* 54:87–143.

Atlas, D. 2001. Functional and physical coupling of voltage-sensitive calcium channels with exocytotic proteins: ramifications for the secretion mechanism. *J Neurochem.* 77:972–985.

Barg, S., J. Galvanovskis, S. Göpel, P. Rorsman, and L. Eliasson. 2000. Tight coupling between electrical activity and exocytosis in mouse glucagon-secreting A-cells. *Diabetes.* 49:1500–1510.

Barg, S., P. Huang, L. Eliasson, D. J. Nelson, S. Obermüller, P. Rorsman, F. Thévenod, and E. Renström. 2001. Priming of insulin granules for exocytosis by granular uptake and acidification. *J. Cell Sci.* 114: 2145–2154.

Bezprozvanny, I, R. H. Scheller, and R. W. Tsien. 1995. Functional impact of syntaxin on gating of N-type and Q-type calcium channels. *Nature*. 378:623–626.

Bokvist, K., L. Eliasson, C. Ämmälä, E. Renström, and P. Rorsman. 1995. Co-localization of L-type Ca^{2+}-channels and insulin-containing secretory granules and its significance for the initiation of exocytosis in mouse pancreatic B-cells. *EMBO J.* 14:505–57.

Bokvist, K., M. Holmqvist, J. Gromada, and P. Rorsman. 2000. Compound exocytosis in voltage-clamped β-cells revealed by carbon fibre amperometry. *Pflügers Arch.* 439:634–645.

Catterall, W. A. 1999. Interactions of presynaptic Ca^{2+} channels and snare proteins in neurotransmitter release. *Ann. N.Y. Acad. Sci. U.S.A.* 868: 144–159.

Cerasi, E. 1992. Aetiology of type II diabetes. *In* Insulin: Molecular Biology of Pathology. F. M. Ashcroft and S. J. H. Ashcroft, editors. IRL Press, Oxford, UK. 352–392.

Detimary, P., P. Gilon, and J. C. Henquin. 1998. Interplay between cytoplasmic Ca^{2+} and the ATP/ADP ratio: a feedback control mechanism in mouse pancreatic islets. *Biochem. J.* 333:269–274.

Eliasson, L., P. Proks, C. Ämmälä, F. M. Ashcroft, K. Bokvist, E. Renström, P. Rorsman, and P. A. Smith. 1996a. Endocytosis of secretory granules in mouse pancreatic beta-cells evoked by transient elevation of cytosolic calcium. *J. Physiol.* 493:755–767.

Fenwick, E. M., A. Marty, and E. Neher. 1982. Sodium and calcium channels in bovine adrenal chromaffin cells. *J. Physiol.* 331:599–635.

Gall, D., J. Gromada, I. Susa, P. Rorsman, A. Herchuelz, and K. Bokvist. 1999. Significance of Na/Ca exchange for Ca^{2+} buffering and electrical activity in mouse pancreatic β-cells. *Biophys. J.* 76:21018–21028.

Gil, A., J. Segura, J. A. Pertusa, and B. Soria. 2000. Monte Carlo simulation of 3-D buffered Ca^{2+} diffusion in neuroendocrine cells. *Biophys. J.* 78:13–33.

Gillis, K. D. 1995. Techniques for membrane capacitance measurements. *In* Single Channel Recording. B. Sakmann and E. Neher, editors. Plenum, New York. 155–198.

Gillis, K. D., and S. Misler. 1992. Single cell assay of exocytosis from pancreatic islet B cells. *Pflügers Arch.* 420:121–123.

Gilon, P., J. Yakel, J. Gromada, Y. Zhu, J. C. Henquin, and P. Rorsman. 1997. G protein-dependent inhibition of L-type Ca^{2+} currents by acetylcholine in mouse pancreatic B-cells. *J. Physiol.* 499:65–76.

Grapengiesser, E., E. Gylfe, and B. Hellman. 1991. Cyclic AMP as a determinant for glucose induction of fast Ca^{2+} oscillations in isolated pancreatic β-cells. *J. Biol. Chem.* 266:12207–12210.

Gromada, J., M. Høy, E. Renström, K. Bokvist, L. Eliasson, S. Göpel, and P. Rorsman. 1999. CaM-kinase II-dependent mobilization of secretory granules underlies acetylcholine-induced stimulation of exocytosis in mouse pancreatic B-cells. *J. Physiol.* 518:745–759.

Grynkiewicz, G., M. Poenie, and R. Y. Tsien. 1985. A new generation of Ca^{2+} indicators with greatly improved fluorescence properties. *J. Biol. Chem.* 260:3440–3450.

Heinemann, C., R. H. Chow, E. Neher, and R. S. Zucker. 1994. Kinetics of the secretory response in bovine chromaffin cells following flash photolysis of caged Ca^{2+}. *Biophys. J.* 67:546–557.

Heinemann, S. H., and F. Conti. 1992. Nonstationary noise analysis and application to patch clamp recordings. *Methods Enzymol.* 207:131–148.

Horrigan, F. T., and R. J. Bookman. 1994. Releasable pools and the kinetics of exocytosis in adrenal chromaffin cells. *Neuron.* 13: 1119–1129.

Klingauf, J., and E. Neher. 1997. Modeling buffered Ca^{2+} diffusion near the membrane: implications for secretion in neuroendocrine cells. *Biophys. J.* 72:674–690.

Lang, J. 1999. Molecular mechanisms and regulation of insulin exocytosis as a paradigm of endocrine secretion. *Eur. J. Biochem.* 259:3–17.

Maeda, H., G. C. Ellis-Davies, K. Ito, Y. Miyashita, and H. Kasai. 1999. Supralinear Ca^{2+} signaling by cooperative and mobile Ca^{2+} buffering in Purkinje neurons. *Neuron.* 24:989–1002.

Martell, A. E., and R. M. Smith. 1974. Critical Stability Constants: Amino Acids (Vol. 1) and Amines (Vol. 2). Plenum, New York.

Nagamatsu, S., Y. Nakamichi, C. Yamamura, S. Matsushima, T. Watanabe, S. Ozawa, H. Furkuwa, and H. Ishida. 1999. Decreased expression of t-SNARE, syntaxin 1, and SNAP-25 in pancreatic β-cells is involved in impaired insulin secretion from diabetic rat islets: restoration of decreased t-SNARE proteins improves impaired insulin secretion. *Diabetes.* 48:2367–2373.

Platzer, J., J. Engel, A. Schrott-Fischer, K. Stephan, S. Bova, H. Chen, H. Zheng, and J. Striessnig. 2000. Congenital deafness and sinoatrial node dysfunction in mice lacking class D L-type Ca^{2+} channels. *Cell.* 102: 89–97.

Renström, E., L. Eliasson, K. Bokvist, and P. Rorsman. 1996. Cooling inhibits exocytosis in single mouse pancreatic B-cells by suppression of granule mobilization. *J. Physiol.* 494:41–52.

Rorsman, P., F. M. Ashcroft, F. M., and G. Trube. 1988. Single Ca channel currents in mouse pancreatic B-cells. *Pflügers Arch.* 412:597–603.

Rorsman, P., L. Eliasson, E. Renström, J. Gromada, S. Barg, and S. Göpel. 2000. The cell physiology of biphasic insulin secretion. *News Physiol. Sci.* 15:72–77.

Rorsman, P., and G. Trube. 1986. Calcium and delayed potassium currents in mouse pancreatic β-cells under voltage-clamp conditions. *J. Physiol.* 374:531–550.

Sakmann, B., and E. Neher. 1995. Geometric properties of pipettes and membrane patches. *In* Single-Channel Recording. B. Sakmann, and E. Neher, editors. Plenum, New York. 637–650.

Seino, S., L. Chen, M. Seino, O. Blondel, J. Takeda, J. H. Johnson, and G. I. Bell. 1992. Cloning of the alpha 1 subunit of a voltage-dependent calcium channel expressed in pancreatic β cells. *Proc. Natl. Acad. Sci. U.S.A.* 89:584–588.

Smith, P. A., F. M. Ashcroft, and C. M. S. Fewtrell. 1993. Permeation and gating properties of the L-type calcium channel in mouse pancreatic β cells. *J. Gen. Physiol.* 101:767–797.

Striessnig, J., M. Grabner, J. Mitterdorfer, S. Hering, M. J. Sinnegger, and H. Glossmann. 1998. Structural basis of drug binding to L Ca^{2+} channels. *Trends Pharmacol. Sci.* 19:108–115.

Takahashi, N., T. Kadowaki, Y. Yazaki, Y. Miyashita, and H. Kasai. 1997. Multiple exocytotic pathways in pancreatic β cells. *J. Cell Biol.* 138: 55–64.

Voets, T. 2001. Dissection of three Ca^{2+}-dependent steps leading to secretion in chromaffin cells from mouse adrenal slices. *Neuron.* 28:537–545.

Voets, T., E. Neher, and T. Moser. 1999. Mechanisms underlying phasic and sustained secretion in chromaffin cells from mouse adrenal slices. *Neuron.* 23:607–615.

von Gersdorff, H., T. Sakaba, K. Berglund, and M. Tachibana. 1998. Submillisecond kinetics of glutamate release from a sensory synapse. *Neuron.* 21:1177–1188.

Wiser, O., M. Trus, A. Hernandez, E. Renström, S. Barg, P. Rorsman, and D. Atlas. 1999. The voltage sensitive Lc-type Ca^{2+} channel is functionally coupled to the exocytotic machinery. *Proc. Natl. Acad. Sci. U.S.A.* 96:248–253.

Wu, M. N., T. Fergestad, T. E. Lloyd, Y. He, K. Broadie, and H. J. Bellen. 1999. Syntaxin 1A interactrs with multiple exocytotic proteins to regulate neuortransmitter release in vivo. *Neuron.* 23:593–605.

Yang, S. N., O. Larsson, R. Bränstrom, A. M. Bertorello, B. Leibiger, I. B. Leibiger, T. Moede, M. Köhler, B. Meister, and P.-O. Berggren. 1999. Syntaxin 1 interacts with the L_D subtype of voltage-gated Ca^{2+} channels in pancreatic β cells. *Proc. Natl. Acad. Sci. U.S.A.* 96: 10164–10169.